Università degli Studi di Padova

Dipartimento di Fisica e Astronomia Galileo Galilei

UNIVERSITÀ DEGLI STUDI DI PADOVA

Dipartimento di Fisica e Astronomia "Galileo Galilei"

Corso di Laurea in Fisica

Tesi di Laurea

Set-up and characterization of a pulsed nuclear magnetic resonance apparatus

Set-up e caratterizzazione di un apparato di risonanza magnetica nucleare

Relatore

Prof.ssa Caterina Braggio

Correlatore

Franco Gonella

Candidato

Marco Frattolillo

Matricola 2000431

Anno Accademico
2023/2024

Abstract

Nuclear Magnetic resonance (NMR) spectroscopy is well known for its wealth of diverse coherent manipulations of spin dynamics, and in time its methods have been adapted to modern experiments in quantum information science to accomplish basic qubit operations. The clearest example of early connections to information theory is the spin echo method, where Hahn demonstrated that inhomogeneous interactions could be refocused to the extent that the phase of the nuclear spins retain information about the local field. In this thesis work, I have participated to the development of a pulsed NMR apparatus, learning about the techniques used to (i) to perturb the nuclei out of alignment with the field and (ii) to measure the small return signal as the misaligned nuclei precess in the field. I have studied the behaviour of hydrogen nuclei in glycerin, where the signal can be easily found and interpreted, by measuring the spin-spin relaxation time.

La spettroscopia a risonanza magnetica nucleare (NMR) è ben nota per la sua capacità di manipolazione della dinamica degli spin e nel tempo è stata adattata agli esperimenti moderni di informazione quantistica per compiere operazioni su quibit. L'esempio principale riguarda il fenomeno dello spin echo, in cui Hahn dimostrò che gli effetti delle interazioni non omogenee del campo magnetico possono essere nuovamente focalizzate per ottenere informazioni riguardanti la relativa disomogeneità. In questo lavoro di tesi, ho partecipato allo sviluppo di un apparato di risonanza magnetica nucleare ad impulsi per lo studio (i) della perturbazione dei nuclei dovuta a un campo magnetico esterno e (ii) alla misura del debole segnale dovuto alla differenza di fase tra i nuclei. Ho analizzato il comportamento degli atomi di idrogeno presenti nella glicerina, dove il risultato è facilmente ottenibile.

Estratto (ITA)

In questo lavoro di tesi, viene trattata la risonanza magnetica nucleare impulsata, come metodo per la manipolazione di sistemi a due livelli.
Consideriamo un sistema di spin che precedono alla frequenza di Larmor in un campo magnetico statico lungo una direzione definita (z). È interessante valutare la dinamica della magnetizzazione complessiva nel campione nel caso in cui venga applicato un ulteriore campo magnetico, ma in questo caso esso sia dipendente dal tempo e applicato sul piano ortogonale al campo statico (lungo x o y). Quest'ultimo campo è realizzato attraverso una bobina orientata lungo uno degli assi x, y. È possibile dimostrare che l'applicazione a tale bobina di impulsi RF di durata definita, consente di ruotare la magnetizzazione di 90° e 180° gradi rispetto alla direzione iniziale. Questa è la fase di controllo della magnetizzazione. In seguito il sistema evolve in base ai tempi caratteristici del sistema, i.e. T_1, T_2 e T_2^*. Il primo contributo tenderà a riportare la magnetizzazione lungo l'asse del campo magnetico principale (*spin-lattice interaction*) mentre gli altri due sono dovuti rispettivamente all'interazioni tra spin (*spin-spin interaction*) e alla disomogeneità del campo magnetico iniziale ΔB. Nel sistema in esame, un campione di glicerina, $T_1 >> T_2$, e condurremo quindi misure di T_2 e T_2^* che permetteranno di stimare il tempo di interazione spin spin e la disomogeneità del campo magnetico nell'apparato sperimentale in esame. Sperimentalmente, otteniamo T_2^* dal segnale di free induction decay osservato in seguito all'applicazione di un impulso $\pi/2$, mentre T_2 è ottenuto attraverso una sequenza di impulsi, tra i quali viene fatto variare il ritardo relativo.
La prima parte di analisi sperimentale si è focalizzata sulla caratterizzazione del circuito RLC con cui è possibile sia applicare gli impulsi RF per il controllo della magnetizzazione, sia rivelare il segnale di induzione che contiene l'informazione riguardante T_2 e T_2^*. In particolare, si misura la frequenza di risonanza del circuito e il relativo fattore di qualità. Quest'ultimo influenza la sensibilità della misura. Una volta nota la risonanza del circuito, si imposta il campo esterno B statico in modo tale che la frequenza di Larmor sia vicina alla risonanza del circuito. La seconda parte verte sulla verifica del corretto funzionamento dell'apparato attraverso la stima di T_2, T_2^* e ΔB utilizzando come campione una soluzione di glicerina e acqua. Nel corso dell'analisi, si è visto come l'apparato presenta delle sistematiche da analizzare ulteriormente, e che determinano un errore significativo su tutti i parametri calcolati. La sistematica principale è dovuta a mismatch di impedenza da risolvere in future realizzazioni del circuito.

Contents

1 Theoretical background

In this section, we lay the theoretical background useful to understand the pulsed NMR. In the first part, it is analyzed the dynamics of a protons in a magnetic field: due to it, the degeneration of the system is removed. To have an induced signal in the coil, is necessary to manipulate the magnetization of the sample using particular pulses length that produces another B-field, orthogonal to precedent one. At the end, it is presented the decoherence effect that are evident after the end of the pulse. The decoherence is described by the Bloch equation and is made by two contributions: the spin-lattice interaction and the spin-spin interaction. In addition, the effects of the B-field inhomogeneity to the system are described, also introducing the possibility to remove them using the spin-echo sequence.

1.1 Protons in magnetic field

To introduce the NMR method, we start by considering the behaviour of a proton in a magnetic field. Using a semi-classical approach, it is possible to formulate the Hamiltonian of the system using the model of a current-currying wire in an external magnetic field.

$$\mathcal{H} = -\vec{\mu} \cdot \vec{B}_0$$

where:

- $\vec{B}_0$ is the external magnetic field imposed. For simplicity, it is assumed to the z-axis $\vec{B}_0 = B_0\hat{z}$
- μ is the magnetic dipole moment defined as:

  $$\vec{\mu} = \frac{e}{2m_p} g_p \vec{S} = \gamma \vec{S}$$

  in which the mass of the proton and its charge are respectively denoted as m_p and e, while γ is the gyro-magnetic ratio.

To resolve the Schrödinger stationary equation, we use the basis of the spin operator indicated as:

$$|+\rangle = \begin{pmatrix} 1 \\ 0 \end{pmatrix} \; |-\rangle = \begin{pmatrix} 0 \\ 1 \end{pmatrix}$$

Therefore the energy is:

$$E = \langle \pm|\mathcal{H}|\pm\rangle = \langle \pm|-\mu \cdot B_0|\pm\rangle = -\gamma B_0 \langle \pm|S_z|\pm\rangle = \mp\frac{1}{2}\hbar\gamma B_0$$

We introduce the Larmor frequency $\omega_0 = \gamma B_0$ thus $E = \mp\frac{\hbar\omega_0}{2}$. This fact makes the system without degeneration, as shown in Figure 1.1.

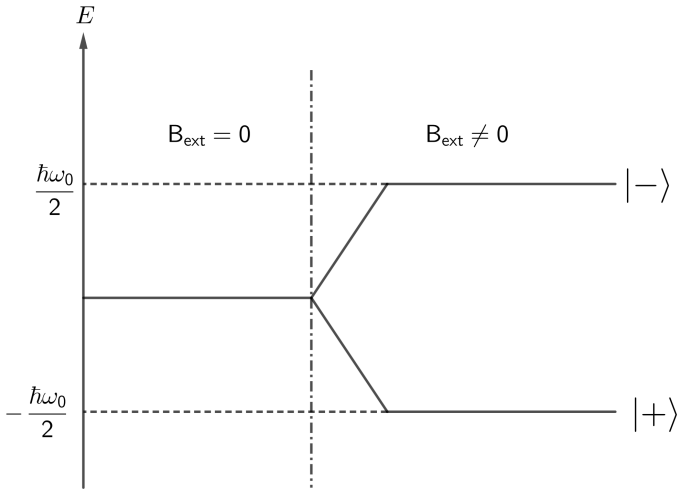

Figure 1.1: The two spin state can not be distinguished when the magnetic field B_0 is zero . when it is applied, the degeneration is removed.

It is also important to consider that there is a certain amount of protons in the substance that depends on volume and density. For this reason, it is important to sum all over the possible protons. Defining the total magnetic dipole moment as:

$$\vec{\mu}_{tot} = \sum_i \gamma \vec{S}_i = \gamma \sum_i \vec{S}_i = \gamma \vec{S}_{tot}$$

To know how many protons contribute to the formation of a net magnetic moment in the sample, we need to consider that protons are in equilibrium with the surroundings making every state populated according to the Boltzmann distribution:

$$N(E) = N_0 e^{-\frac{E}{k_B T}}$$

There are two possible states:

$$N(+) = \frac{N_0}{2} e^{\frac{\hbar\omega_0}{2k_B T}}$$

$$N(-) = \frac{N_0}{2} e^{\frac{-\hbar\omega_0}{2k_B T}}$$

where N_0 is the number of proton in the sample. The ratio of the two population is:

$$\frac{N(+)}{N(-)} = e^{\frac{3\hbar\omega_0}{2k_B T}}$$

If it is assumed that $\hbar\omega_0 << k_B T$, it is possible to make a first-order Taylor expansion of the exponential obtained:

$$\frac{N(+)}{N(-)} \approx \left(1 + \frac{3}{2}\frac{\hbar\omega_0}{k_B T}\right)$$

From the expression above, it is clear that N (+) is greater than N (+) and so there are only some spins that are aligned to magnetic field. As a consequence there is a non zero total magnetic dipole moment, defined as:

$$\vec{M} = \frac{\vec{\mu}}{V}\gamma\frac{\hbar}{2}\frac{(N(+) - N(-))}{V}\hat{z}$$

Consequently:

$$N_a = N(+) - N(-) = \frac{N_0}{2}\left[\exp\left\{\frac{\hbar\omega_0}{2k_BT}\right\} - \exp\left\{\frac{-\hbar\omega_0}{2k_BT}\right\}\right] \approx \frac{N_0}{2}\frac{h\omega_0}{k_BT}$$

and so, if in a sample there a N atoms, the N_0 number of proton is multiplied to to atomic number Z. Finally:

$$M_0 = \frac{\hbar^2\gamma^2 B_0}{4k_BT}\frac{Z\rho N_A}{mm_g}V_{sample}$$

where mm_g is the molecular weight, ρ and V_{sample} are respectively the density and volume of the sample while N_A is the Avogadro's number.
It is interesting to have a graphical view of the system, presented in Figure 1.2. Newton's law of the system is:

$$\frac{d\vec{S}_{tot}}{dt} = \vec{\mu}_{tot} \wedge \vec{B}_0$$

or in terms of net magnetization $\vec{M}$:

$$\frac{d\vec{M}}{dt} = \gamma\vec{M} \wedge \vec{B}_0 = \omega_0\vec{M} \wedge \hat{z}$$

which is the Newton's equation for a clockwise precession around z-axis at ω_0 angular speed.

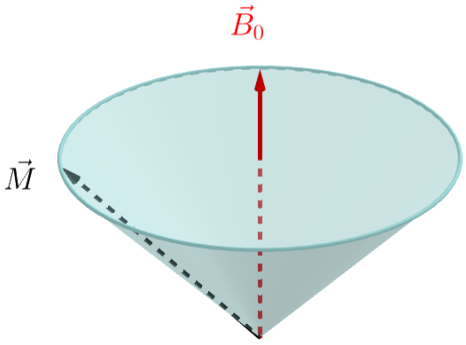

Figure 1.2: Precession of $\vec{M}$ around $\vec{B}_0$.

1.2 Pulsed NMR in classical mechanics

To measure the effect of the external magnetic field on the sample, it is possible to put the sample in a coil and measure the induced signal on it. However, the net magnetization is along the z-axis and therefore parallel to the normal vector of the coil, making impossible to have an induced signal. To avoid this issue, it is necessary to change the angle between them and this can be obtained by applying a variable magnetic field orthogonal to the other one $\vec{B}_1(t) = B_1 \cos\omega t\hat{x}$. This new field is produced by a coil thanks to a RF signal: its length is proportional to the angle that has been made by the magnetization. A graphical view of the situation is given in Figure

1.3.

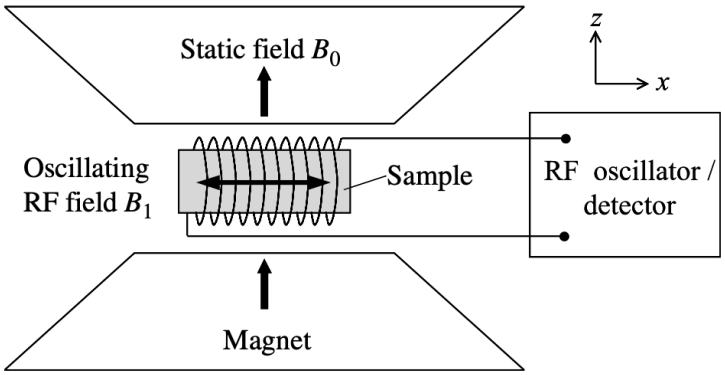

Figure 1.3: Experimental setup with the two different magnetic fields: the one produced by the RF signal along the x-axis and the static magnetic field along the z-axis. In this configuration, it is possible to change the magnetization's direction, having an induced signal in the coil.

The dynamics equation of the motion with the new magnetic field is now:

$$\frac{d\vec{M}}{dt} = \gamma\vec{M} \wedge \left(\vec{B}_0 + \vec{B}_1\right) = \gamma\vec{M} \wedge \vec{B}$$

which corresponds to a double precession, one along $\vec{B}_0$ and the other along $\vec{B}_1$. The representation is in Figure 1.4 where it is highlighted that to the angle α(red in Figure 1.4) between the magnetisation vector and the z-axis is no longer conserved due to $\vec{B}_1$.

The study of system's dynamics in the lab frame is quite complex, for this reason we move in the frame that rotates clockwise around at the same angular frequency of the RF signal. The new coordinates are now called x',y',z' and they are connected to the previous one thanks to the equations below:

$$\hat{x}' = \cos\omega t\hat{x} - \sin\omega t\hat{y}$$

$$\hat{y}' = \cos\omega t\hat{x} + \sin\omega t\hat{y}$$

$$\hat{z}' = \hat{z}$$

Writing $\vec{B}_1$ as superposition of two counter-rotating magnetic fields to simplify the calculation in the rotating frame:

$$\vec{B}_r(t) = \frac{B_1}{2}\left(\cos\omega t\hat{x} + \sin\omega t\hat{y}\right)$$

$$\vec{B}_l(t) = \frac{B_1}{2}\left(\cos\omega t\hat{x} - \sin\omega t\hat{y}\right)$$

which became in the new frame:

$$\vec{B}_r = \frac{B_1}{2}\left(\cos 2\omega t\hat{x}' + \sin 2\omega t\hat{y}'\right)$$

$$B_l(t) = \frac{B_1}{2}\hat{x}'$$

while $\vec{B}_0$ is still the same:

$$\vec{B}_0 = B_0\hat{z}'$$

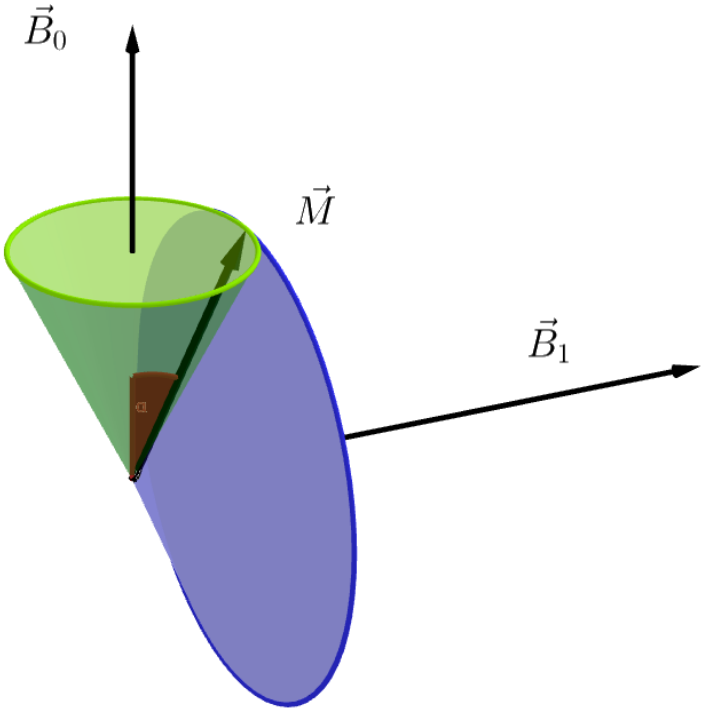

Figure 1.4: Graphical representation of the two precession: the first is the green one along $\vec{B}_0$ and the other along $\vec{B}_1$ in purple. In contrast to the previous case, the angle red α is no longer conserved.

Remembering the Poisson's equation for a general vector $\vec{v}$:

$$\frac{d\vec{v}}{dt} = \left(\frac{d\vec{v}}{dt}\right)' + \vec{\omega} \wedge \vec{v}$$

Applying it to the magnetization vector, the new dynamics equation is:

$$\left(\frac{d\vec{M}}{dt}\right)' = \gamma\vec{M} \wedge \left(\vec{B}_0 + \vec{B}_1 + \frac{\vec{\omega}}{\gamma}\right) = \gamma\vec{M} \wedge \vec{B}_{eff}$$

With $\vec{B}_{eff}$:

$$\vec{B}_{eff} = \begin{pmatrix} \frac{B_1}{2}(1 + \cos(2\omega t)) \\ \frac{B_1}{2}\sin 2\omega t \\ B_0 - \frac{\omega}{\gamma} \end{pmatrix}$$

If the RF angular frequency is the same as the precession frequency ω_0, the third component of $\vec{B}_{eff}$ is zero. In addition, the terms sine and cosine have a very high frequency (2ω): therefore, their period is very long compared to that of the Larmor precession, so they can be neglected. Newton's equation is:

$$\left(\frac{d\vec{M}}{dt}\right)' = \gamma\vec{M} \wedge \frac{B_1}{2}\hat{x}'$$

which is a clockwise precession around the x'-axis at an angular frequency Ω called Rabi frequency.

$$\Omega = -\frac{\gamma B_1}{2}$$

Using this description, it is possible to visualise the spin manipulation. If the magnetization is initially aligned with the z-axis, the application of a $\pi/2$ RF pulse allows it to rotate by 90°, producing an induced signal in the coil. The duration of this pulse t_{90} is set by the amplitude of the B_1 field applied through the coil:

$$\Omega = \frac{\frac{\pi}{2}}{t_{90}} \Rightarrow t_{90} = \frac{\pi}{\gamma B_1}$$

Similarly, it is possible to flip the magnetization of π angle using a pi-pulse that lasts:

$$t_{180} = 2t_{90} = \frac{2\pi}{\gamma B_1}$$

In Figure 1.5 there is a graphical view of the effect on the magnetization made by a π and $\pi/2$ pulse:

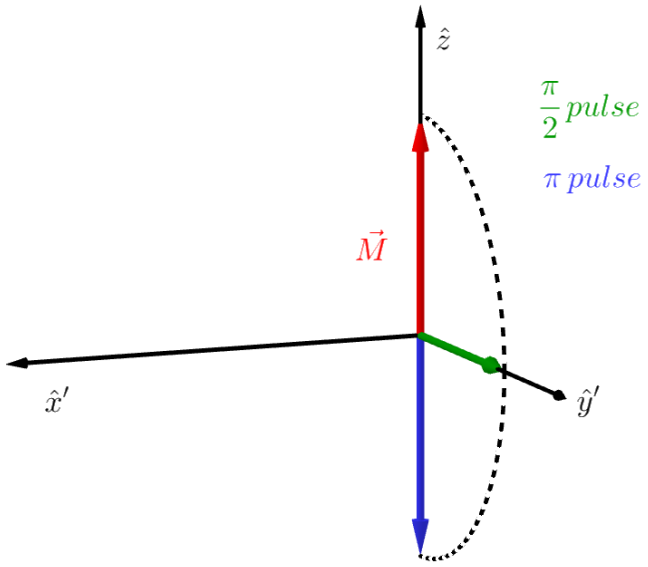

Figure 1.5: Graphical view of the new direction of the magnetization after a $\pi/2$ pulse, which changes $\vec{M}$ of 90°, and π that flips it.

1.3 Pulsed NMR in quantum mechanics

Beyond the classic explanation of pulsed NMR, there is a quantum mechanic description that predicts the same dynamics. The following discussion is taken from [3].
Considering the same situation in the classic view represented in Figure 1.3. There are two possible ways to resolve this problem:

- Treat the presence of $\vec{B}_1$ as a perturbation because its intensity is smaller than $\vec{B}_0$ and use Fermi's second golden to determine the transition probability.
- Use the symmetry formalism of quantum mechanics in a similar way to the classical explanation.

To have a complete view, it's better to analyze the second option.
Writing the Hamiltonian of the system using the same consideration of section 1.1:

$$\mathcal{H} = -\gamma \frac{\hbar}{2}(\sigma_x B_1 + \sigma_z B_0)$$

where the σ_i are the Pauli's matrix defined as below:

$$\sigma_1 \equiv \sigma_x \equiv \begin{pmatrix} 0 & 1 \\ 1 & 0 \end{pmatrix} \qquad \sigma_2 \equiv \sigma_y \equiv \begin{pmatrix} 0 & -i \\ i & 0 \end{pmatrix} \qquad \sigma_3 \equiv \sigma_z \equiv \begin{pmatrix} 1 & 0 \\ 0 & -1 \end{pmatrix}$$

In matrix form:

$$\mathcal{H} = -\gamma \frac{\hbar}{2} \begin{pmatrix} B_0 & \frac{B_1}{2} e^{i\omega t} \\ \frac{B_1}{2} e^{-i\omega t} & -B_0 \end{pmatrix} = -\frac{\hbar}{2} \begin{pmatrix} \omega_0 & \tilde{\omega} e^{i\omega t} \\ \tilde{\omega} e^{-i\omega t} & -\omega_0 \end{pmatrix}$$

Where $\vec{B}_1 = B_1 \cos(\omega t) = \frac{B_1}{2}\left(e^{i\omega t} + e^{-i\omega t}\right)$,$\omega_0 = \gamma B_0$ and $\tilde{\omega} = \frac{1}{2}\gamma B_1$.
First of all, it has been assumed a zero $\vec{B}_1$ and the superimposition of the wave function:

$$\left|\psi\right\rangle = c\left|+\right\rangle + d\left|-\right\rangle$$

The time evolution of ψ is described by the Schrödinger equation:

$$H\left|\psi\right\rangle = i\hbar \frac{\partial \psi}{\partial t} \Rightarrow \begin{pmatrix} \dot{c} \\ \dot{d} \end{pmatrix} = \frac{i}{2} \begin{pmatrix} \omega_0 & 0 \\ 0 & -\omega_0 \end{pmatrix} \begin{pmatrix} c \\ d \end{pmatrix}$$

and so:

$$c(t) = c_0 e^{\frac{i}{2}\omega t}$$

$$d(t) = d_0 e^{-\frac{i}{2}\omega t}$$

And if $\vec{B}_1 \neq 0$ the solutions are now:

$$c(t) = \tilde{c(t)} e^{\frac{i}{2}\omega t}$$

$$d(t) = \tilde{d(t)} e^{-\frac{i}{2}\omega t}$$

where for $\omega \to 0$ the limits for $\tilde{c(t)}$ and $\tilde{d(t)}$ are c(0) and d(0) respectively.
Moving from the laboratory frame to a rotating frame around the z-axis with angular frequency ω, the same as $\vec{B}_1$, the unitary operator is:

$$U(t) = e^{-i/2\omega t \sigma_z} = \begin{pmatrix} e^{-\frac{i}{2}\omega t} & 0 \\ 0 & e^{\frac{i}{2}\omega t} \end{pmatrix}$$

Using the Wigner's theorem that prescribes the new Hamiltonian $\mathcal{H}$ and wave function ψ':

$$\psi'(t) = U(t)\psi(t)$$

$$\mathcal{H}' = U(t)\mathcal{H}U(t)^{\dagger}$$

Assuming newly the superimposition on the wave function:

$$\psi'(t) = \overline{c}(t)\left|+\right\rangle + \overline{d}(t)\left|-\right\rangle$$

so the equation between the coefficient in the lab frame and the rotating frame is:

$$\begin{pmatrix} \overline{c} \\ \overline{d} \end{pmatrix} = \begin{pmatrix} e^{-\frac{i}{2}\omega t} & 0 \\ 0 & e^{\frac{i}{2}\omega t} \end{pmatrix} \begin{pmatrix} c \\ d \end{pmatrix}$$

To reconstruct $\mathcal{H}'$, it is possible to use the equation above because:

$$\frac{d\overline{c}}{dt} = \frac{d}{dt}\left(e^{-\frac{i}{2}\omega t}c\right) = \frac{e^{-i/2\omega t}}{2}(-i\omega c + 2\dot{c})$$

where the expression of c and $\dot{c}$ is known from the upper consideration. Similarly, for $\overline{d}$. The new Hamiltonian is now:

$$\mathcal{H}' = \frac{\hbar}{2}\begin{pmatrix}\Delta\omega & -\tilde{\omega}\\ -\tilde{\omega} & -\Delta\omega\end{pmatrix}$$

where $\Delta\omega = \omega_0 - \omega$. First of all, it's noticed that $\mathcal{H}'$ can be written as:

$$\mathcal{H}' = -\frac{\hbar}{2}\gamma\left(\frac{\tilde{\omega}}{\gamma}\sigma_x - \frac{\omega_0 - \omega}{\gamma}\sigma_z\right) = -\vec{\mu}\cdot\vec{B}_{eff}$$

where $\vec{B}_{eff} = \frac{\tilde{\omega}}{\gamma}\hat{x} - \left(B_0 + \frac{\omega}{\gamma}\right)\hat{z}$
The Hamiltonian that is obtained is the same as the one treated in section 1.1: the only difference is that $\vec{B}_{eff}$ is in a particular direction in the (x,z) plane. Noticed that:

$$\mathcal{H}' = -\frac{\hbar}{2}\sqrt{(\Delta\omega^2 + \tilde{\omega}^2)}\left[-\frac{\Delta\omega}{\sqrt{(\Delta\omega^2 + \tilde{\omega}^2)}}\sigma_z + \frac{\tilde{\omega}}{\sqrt{(\Delta\omega^2 + \tilde{\omega}^2)}}\sigma_x\right] = -\frac{\hbar}{2}\sqrt{(\Delta\omega^2 + \tilde{\omega}^2)}(\vec{\sigma}\cdot\hat{n})$$

where $\hat{n}$ is the versor of $\vec{B}_{eff}$. Remembering the spin properties:

$$\sigma\cdot\hat{n}\,|\pm\hat{n}\rangle = \pm|\pm\hat{n}\rangle$$

The energy of the system is now easy to find:

$$E = \langle\pm\hat{n}|\mathcal{H}'|\pm\hat{n}\rangle = \mp\frac{\hbar}{2}\sqrt{(\Delta\omega^2 + \tilde{\omega}^2)} = \mp\frac{\hbar}{2}\Omega$$

where Ω is called the Rabi angular frequency. Think back to the definition of $\hat{n}$:

$$|+\hat{n}\rangle = \cos\frac{\theta}{2}|+\rangle + \sin\frac{\theta}{2}|-\rangle$$

$$|-\hat{n}\rangle = -\sin\frac{\theta}{2}|+\rangle + \cos\frac{\theta}{2}|-\rangle$$

and in this case:

$$cos(\theta) = -\frac{\Delta\omega}{\sqrt{(\Delta\omega^2 + \tilde{\omega}^2)}} \quad sin(\theta) = \frac{\tilde{\omega}}{\sqrt{(\Delta\omega^2 + \tilde{\omega}^2)}}$$

For the reason mentioned before, the first assumption to do is having a initial state $|\psi_0'\rangle = |+\rangle$. The time-evolution of this wave vector is:

$$|\psi'(t)\rangle = \exp\left(-\frac{i}{\hbar}\mathcal{H}'t\right)|+\rangle = \exp\left(-\frac{i}{\hbar}\mathcal{H}'t\right)|+\hat{n}\rangle\langle+\hat{n}|+\rangle + \exp\left(-\frac{i}{\hbar}\mathcal{H}'t\right)|-\hat{n}\rangle\langle-\hat{n}|+\rangle =$$

$$= \exp\left(i\frac{\Omega}{2}t\right)\cos\frac{\theta}{2}|+\hat{n}\rangle - \sin\frac{\theta}{2}\exp\left(-i\frac{\Omega}{2}t\right)|-\hat{n}\rangle$$

Coming back to laboratory frame:

$$|\psi(t)\rangle = U^{\dagger}|\psi'(t)\rangle = \begin{pmatrix}e^{\frac{i}{2}\omega t}\left[\cos\frac{\Omega}{2}t + i\cos\theta\sin\frac{\omega}{2}t\right]\\ e^{-\frac{i}{2}\omega t}i\sin\theta\sin\frac{\Omega}{2}t\end{pmatrix}$$

So the probability P_+ to find the spin with the same wave function is:

$$P_+ = \left|\langle +|\psi(t)\rangle\right|^2 = \cos^2\frac{\Omega}{2}t + \cos^2\theta\sin^2\frac{\Omega}{2}t$$

and therefore the probability to find the inverted spin is:

$$P_-(t) = \left|\langle -|\psi(t)\rangle\right|^2 = 1 - P_+ = \frac{\tilde{\omega}^2}{\Delta\omega^2 + \tilde{\omega}^2}\sin^2\left(\frac{t}{2}\sqrt{\Delta\omega^2 + \tilde{\omega}^2}\right)$$

Graphing the amplitude of P_-:

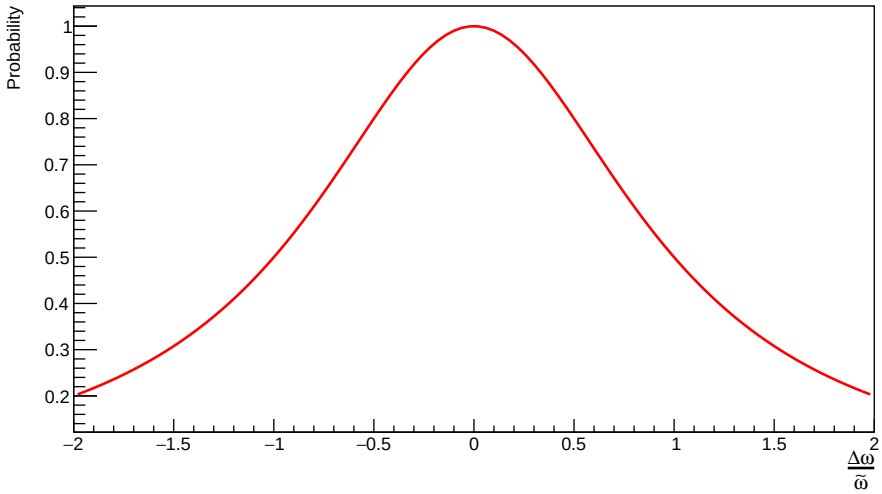

Figure 1.6: Graph of P_- amplitude. It's value is maximum when $\omega = \omega_0$, also called resonant condition.

Analyzing Figure 1.6, it is possible to see that for $\omega = \omega_0$ the probability amplitude is maximum. This condition is called resonance condition. In this situation the wave function is:

$$\left|\psi(t)\right\rangle = \cos\left(\frac{\tilde{\omega}t}{2}\right)|+\rangle + isin\left(\frac{\tilde{\omega}t}{2}\right)|-\rangle = e^{-\frac{\sigma_x}{2}\tilde{\omega}t}|+\rangle$$

which exactly correspond to a rotation of the wave vector $|+\rangle$ around the x-axis and if the $\theta = \tilde{\omega}t$ angle rotation is chosen to be $\pi/2$ or π we obtain respectively the $\pi/2$ pulse and π pulse; the same as the one obtained using the classical mechanics.

1.4 Decoherence

As detailed in the previous sections, it is possible to manipulate the magnetization using resonant pulses. Once the control pulse ends, the interaction of the two-level system with the environment takes a primary role in the dynamics, and the decoherence effects can be observed. Decoherence is a quantum mechanics effect that consists of losing information on the system. It is made by two different effects:

- dephasing
- relaxation to the ground state

The following description is inspired from [9].
As an example, considering a pure state $|+\rangle = \frac{1}{\sqrt{2}}(|0\rangle + |1\rangle)$ where $|0\rangle$,$|1\rangle$ are the basis of spin.

The associated density operator is:

$$\rho = \begin{pmatrix} 1 & 0 \\ 0 & 0 \end{pmatrix}$$

The state is pure due to its trace, which is equal to one. In the spin basis, the density operator is :

$$\rho = |+\rangle \langle +| = \frac{1}{2} \begin{pmatrix} 1 & 1 \\ 1 & 1 \end{pmatrix}$$

Applying the time evolution, the density operator at a time t became:

$$\rho(t) = \frac{1}{2} \begin{pmatrix} 1 & e^{i\omega t} \\ e^{-i\omega t} & 1 \end{pmatrix}$$

where ω is the action of a general spin Hamiltonian. The first consequence of the time evolution is the oscillation of the probability amplitude in the $|+\rangle$ state:

$$\langle |+\rangle | \rho(t) || + \rangle \rangle = \frac{1}{2}(1 + \cos \omega t)$$

Including the dephasing and relaxation to the ground, the ρ change:

$$\rho(t) = \frac{1}{2} \begin{pmatrix} 2 - e^{-\gamma_1 t} & e^{i\omega t - \gamma_2 t} \\ e^{-i\omega t - \gamma_2 t} & e^{-\gamma_1 t} \end{pmatrix}$$

The first modifies the probability of finding $|+\rangle$, introducing an exponential decay with γ_2 as parameter while the second one involves the possibility, if the $|1\rangle$ has a larger energy than $|0\rangle$, there could be spontaneous emission that drives the system to the ground state. This process is regulated by γ_1.
In the pulsed NMR, the term associated with the relaxation to the ground is due to spin-lattice interaction which tends to restore the Maxwell-Boltzmann distribution, which causes the system to be at the lowest energy level. This process is characterized by the decay constant $T_1 (= \gamma_1^{-1})$. The dephasing term is instead associated to the spin-spin interaction that is described by $T_2 (= \gamma_2^{-1})$. In terms of magnetization vector, decoherence is described by the Bloch equation presented in [2] by Bloch:

$$\frac{d\vec{M}}{dt} = -\vec{B}(t) \wedge \vec{r}(t) - \frac{1}{T_1}(r_z(t) - r_z(0))\hat{z} - \frac{1}{T_2}\left(r_x(t)\hat{x} + r_y(t)\hat{y}\right)$$

where $\vec{r}(t)$ is the state vector on the Bloch sphere. A graphical description of the Bloch equation is given in Figure 1.7.

1.4.1 Spin-lattice interaction

A first contribution to this effect is made by the lattice of the sample. In the section before, it has been said that the majority of the spin tend to be aligned with z-axis (the direction of the magnetic field). However, applying a pulse could change the magnetization. The spin-lattice interaction acts to restore the magnetization along the z-axis. The equation that described this mechanism is the following one and its parameter T_1 is called spin-lattice time:

$$M_z(t) = M_0 + \left(M_i - M_0 e^{-\frac{t}{T_1}}\right)$$

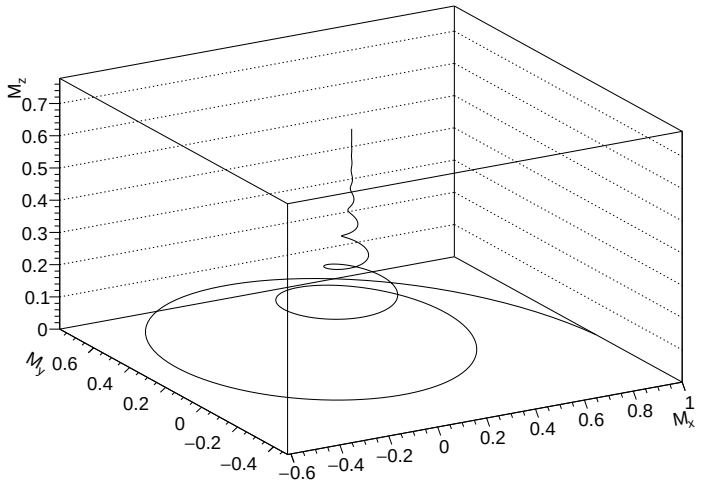

Figure 1.7: Graphical representation of the magnetization following the Bloch's equation. Applying a $\pi/2$ pulse the magnetization is completely along the y-axis, immediately after, due to the interaction with the surroundings, the x-y magnetization start to decrease (spin-spin interaction) while the z-component start to increase (spin-lattice interaction).

where M_i is the initial perturbed longitudinal magnetization while M_0 the one along the z-axis without perturbation. As an example, if a $\pi/2$ pulse is applied to the sample, the magnetization is transferred from the z-axis to the y-axis ($M_i = 0$) and so the equation that describes this phenomena is :

$$M_z(t) = M_0\left(1 - e^{-\frac{t}{T_1}}\right)$$

The π pulse instead flips the magnetization making $M_i = -M_0$. The Bloch's equation is the following one:

$$M_z(t) = M_0\left(1 - 2e^{-\frac{t}{T_1}}\right)$$

1.4.2 Spin-spin interaction

The spin-spin interaction can be classically explained by considering that proton produces a local magnetic field $\vec{B}_{local}$ that can affect neighboring nucleus. The overall magnetic field a proton is subject is:

$$\vec{B'} = \vec{B}_{eff} + \vec{B}_{local}$$

$\vec{B}_{local}$ can be calculated using the formula for a magnetic field generated by a dipole:

$$B_{local} \approx \left(\frac{\mu_0}{4\pi}\right)\frac{\mu_n}{r^3} \approx 5 \cdot 10^{-4}\mathrm{T}$$

The obtained value above is just an maximum measurement, there will be some protons that are effected on a bigger local magnetic field while other subjected to a minor one, producing precessions with different angular frequencies.
The time evolution of the envelope transverse (x-y plane) magnetization is characterized by the following equation:

$$M_{x,y} = M_{x,y;0}e^{-\frac{t}{T_2}}$$

where T_2 is called the spin-spin relaxation time. In general, T_1 is much longer than T_2 and for this reason in a first approximation the spin-lattice contribution can be negligible.

1.4.3 Field inhomogeneity and FID

The effect of B_0 inhomogeneity consists of increasing or decreasing the angular frequency of each proton, like the spin-spin interaction.
After the application $\pi/2$ pulse, the RF signal decays exponentially with decay constant $1/T_2^*$:

$$\frac{1}{T_2^*} = \frac{1}{T_1} + \frac{1}{T_2} + \gamma \Delta B_0$$

where ΔB_0 represents the magnetic field inhomogeneity. The time evolution of the FID is:

$$M_{x,y} = M_{x,y;0} e^{-\frac{t}{T_2^*}}$$

1.4.4 The spin-echo sequence

To evaluate the effect of the spin-spin interaction, it is important to remove the contribution of the field inhomogeneity ΔB that is the most important parameter in the FID. This problem was overcome by Hanh, who created a particular pulse sequence, called spin-echo.
This pulse sequence is made of a $\pi/2$ pulse and, after a delay τ, a π pulse. The physical mechanism of the spin-echo sequence is presented in Figure 1.8.

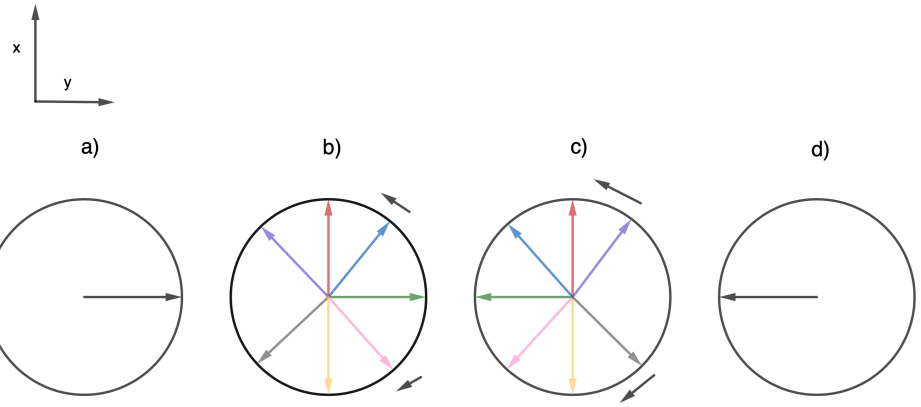

Figure 1.8: Physical mechanism of pulse sequence: in a) there is the total magnetization along the y-axis after applying a $\pi/2$ pulse. b) due to the field inhomogeneity, magnetizations start to fan out with different angulary frequency. c) at t=τ the π pulse is applied, making the spins reversed with the same angular frequency as before. d) the spins are newly completely in phase along the -y-axis.

As it is possible to see in Figure 1.9, the are two maximum: the first one is the one obtained immediately after the $\pi/2$ pulse while the second one, after the π pulse, is reduced on amplitude only for the spin-spin interaction. Changing τ between the two pulses is possible to obtain some points to verify the Bloch Equation for $M_{x,y}$ in which t=2τ. This method will be used later to measure the spin-spin time T_2 in the glycerin sample.
Using Hahn's metaphor presented in [7]:

> *Let a team of runners with different but constant running speeds start at a time t = 0 as they would at a track meet... At some time T these runners would be distributed around the race track in apparently random positions. The referee fires his gun at a time t = τ > T, and by the previous arrangement, the racers quickly turn around and run in the opposite direction with their original speeds. Obviously, at a time t = 2τ , the runners will return together precisely at the starting line.*

As already said, the spin-echo technique allows to eliminate the effect of the field inhomogeneity, leaving only the effects related to T_1 and T_2. In Hahn's word:

> *The decay of the echo may be understood in terms of the race track analogy if it is assumed now that the runners become fatigued after the start of the race. For this reason, they may change their speeds erratically or even drop out of the race completely. Consequently, following the second gun shot (the second pulse), some of the racers may return together at the starting line, but not all of them.*

An example of the spin-echo sequence is in the following picture:

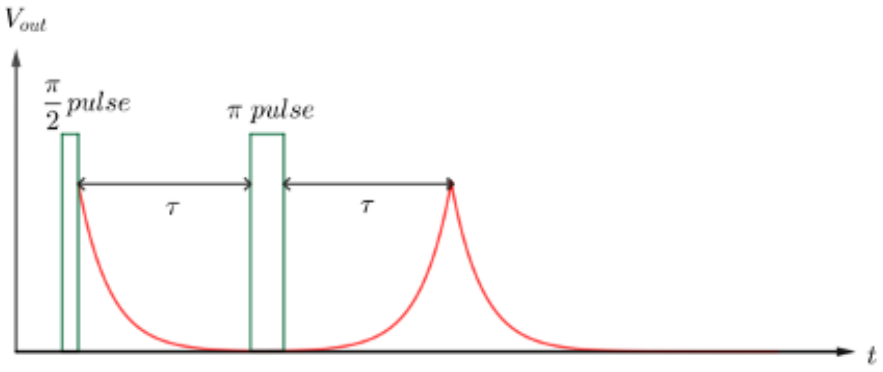

Figure 1.9: An example of spin-echo sequence: after applying a $\pi/2$ pulse there is the FID. Waiting a time τ, it is applied the π pulse which permits to reconstruct the maximum value of the magnetization at t=2τ without the effect of the field inhomogeneity.

2

Experimental setup

The focus of this thesis work is to set-up an experimental apparatus to measure T_1 and T_2 in NMR materials. The experimental setup, shown in Figure 2.2, is inspired to the one introduced by G.Gabrielse and his collaborators to build a He-3 NMR probe [5] .
In this setup, it is possible to both excite the material and readout the NMR signal through the same circuit by using a solid state switch. To test the apparatus, a glycerin sample is employed.

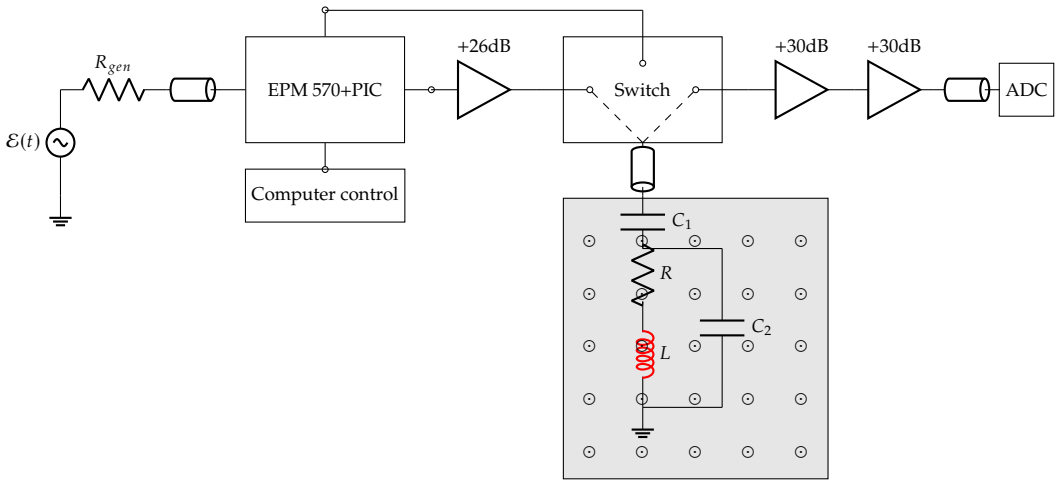

Figure 2.1: This is the electronic circuit used to excite the NMR sample and read out the induced signal.The sample is inside the coil of the RLC circuit (shown in red).

2.1 RLC circuit

The core of the set-up is the RLC circuit in which the inductance $L \approx 1.1\mu$H is made of copper wire wound around the NMR sample (10 turns) and the resistance $R \approx 2\Omega$ is intrinsic on the wire. In the circuit there are two capacitor: C_2 is about 40pF while C_1 is chosen to be variable, allowing impedance matching. Its value is $C_1 \approx 14$pF.
As it is a resonant circuit, to maximize the energy transfer between the driving circuit and the sample, two conditions need to be met:

- The Larmor frequency ν_0 coincides with the resonant frequency of the circuit ν_{RLC}
- The circuit at resonance has the same impedance of the transmission line (50 MΩ)

The set-up shown in Figure 2.2 has been devised to measure the bandwidth, the resonant frequency and the matching.

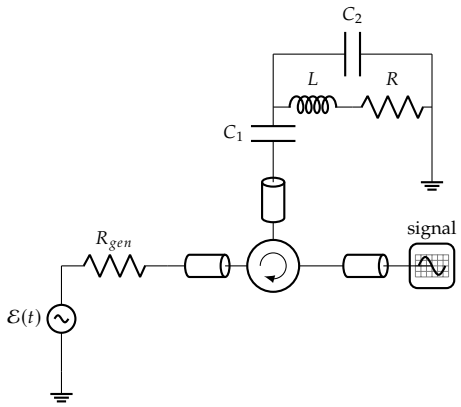

Figure 2.2: Schematic view of the circuit used to measure the ν_{RLC} and bandwidth of the RLC circuit.

An RF pulse is sent from the generator to the RLC circuit and the fraction of power reflected by the circuit is measured at the reflection port of the directional coupler. At resonance, the power reflected is minimum. In addition, as depicted in Figure 2.3, the good matching condition is obtained when the initial and final peak, at the start and end of the RF pulses, respectively, have comparable amplitudes. This is quantified by the coefficient $\beta = \frac{P_{line}}{P_{RLC}}$.
The exponential decay observed when $\beta \approx 1$ is used to infer the quality factor of the circuit $Q = \frac{\nu}{\Delta\nu}$ is approximated to $Q = \pi\tau\nu_{RLC}$, with τ exponential decay constant.

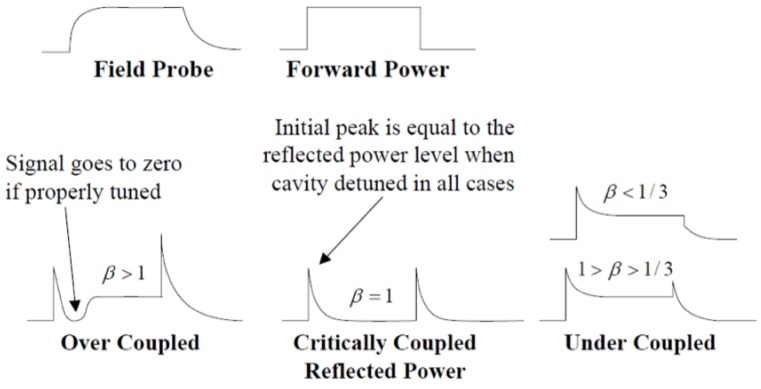

Figure 2.3: Effects of the impedance matching [images take from page 65 of RF Theory and Design - Notes, Jeremiah Holzbauer] .

In the set-up used in the present thesis, this procedure is realized using RF pulses are generated by a pulse generator (mod. 50 MHz Hewlett-Packard) connected to a signal generator (mod.Rhode& Schwartz SMT 06). Comparing Figure 2.3 and the experimental resulted shown in 2.4, it is clear that the system is in over-coupling condition (β>1).

Figure 2.4: Oscilloscope view of the measurement.

Once the sample set in place, the frequency of resonance is perturbed due to the permeability of the NMR sample, thus in the following paragraphs measurements are reported for both the cases (i.e. with and w/o the sample).

Resonant frequency without sample

The frequency that minimises the amplitude of the reflected signal is found at **21,010** MHz. The measurement of τ can be obtained by making a linear fit to the logarithm of the data, as shown in Figure 2.5.

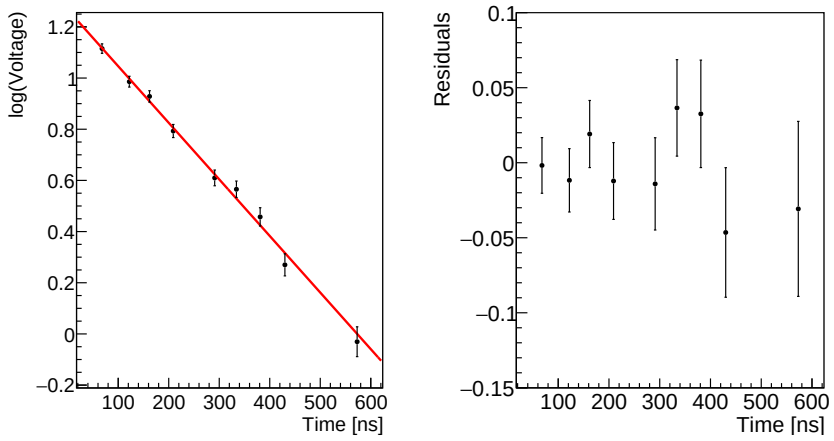

Figure 2.5: Linear fitting and residual for measurement of RLC's τ without the sample of glycerin inside the coil.The exponential fit has been linearized to obtain statistical uncertain on parameter.

There is a good match between the linear fit and the data with $\tau = (454 \pm 21)$ns where the uncertain is given by the fit. Calculated Q-factor is $Q = 30 \pm 1$ which corresponds to a band with of 0.7 MHz.

Resonant frequency with sample

In the circuit including the glycerin sample, the frequency that minimizes the reflected signal is **20.740** MHz. Related fit and data are reported in Figure 2.6.

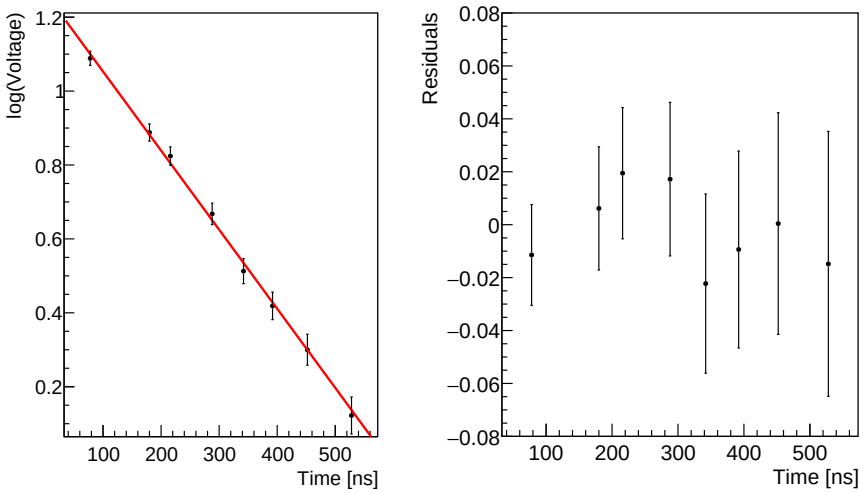

Figure 2.6: Linear fit and residual for measurement of RLC's τ with the sample of glycerin.

In this case, $\tau = (476 \pm 23)ns$ is obtained, with a quality factor of $Q = 31 \pm 1$.
Clearly, there is a difference between this two frequencies due to the presence of the NMR sample but the interesting fact is the compatibility between the two τ. This means a similar lost of RF signal; surprisingly considering the presence of the sample in the second configuration.

A practical approach to determine the resonance frequency in pulsed NMR

As it will be detailed in the following, during the spin echo sequence, we observed that the maximum amplitude of the echo is obtained for a frequency that differs slightly to the precedent one (ν_0 = 20.740MHz), as reported in table 2.1

Table 2.1: Different values of resonant frequency: the first one is obtained from RF pulses measured in reflection while the second one is characterized by the maximum amplitude of the spin-echo.

	ν_{RLC} [MHz]
Measurement with RF pulses	20.740
Spin-echo	20.741

2.2 Sample and B field

The static B field that magnetises the sample is obtained by running a few Ampere through an electromagnet (EM) (mod. Bruker Magnet B-E 15). The B vs. I curve for different distances between the magnet poles is shown in Figure 2.7.

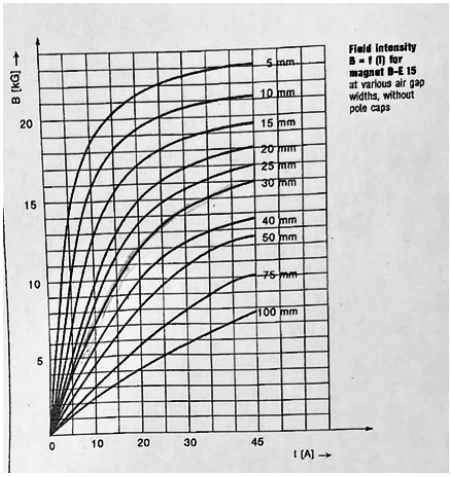

Figure 2.7: Graph of magnetic field produced vs current with different space between poles.

During this thesis work, the distance between the EM poles is set to 30 mm. To overlap the Larmor frequency of the sample with ν_{RLC}, the amplitude of the B-field must be:

$$\nu_0 = \nu_{RLC} \Rightarrow B_{ext} = \frac{\nu_0}{\tilde{\gamma}} = 0.487\,\mathrm{T}$$

where $\tilde{\gamma} \approx 42.5756$MHz/T, defined in section 1.1.
As shown in Figure 2.7, this B-field can be obtained by setting a current of about 8 A at the EM.The precise value of current is set by measuring the field with a Hall probe. We thus set $B = (0.4870 \pm 0.0003)$T corresponding to a current of 7.832 A.
The NMR sample is a solution of water and glycerin ($C_3H_80_3$) and the maximum power that can be induced in the coil is:

$$P = \frac{(\hbar\omega_0^2)}{2k_BT}\frac{Z\rho N_A}{mm_g}V_{sample}$$

where it has been assumed that Z=8, mm_g=92.09382 g/mol, $\rho = 1.26\,g/cm^3$ and volume $V_{sample} = (0.8 \pm 0.1)\mathrm{cm}^3$. Assuming the uncertain of ω_0 negligible, the stored energy is $E = (2.2 \pm 0.3) \cdot 10^{12}$eV/s $= (3.5 \pm 0.5) \cdot 10^{-7}$W. This value is very small considering that to excite the NMR sample is used power of mW.

2.3 Digital pulse programmer

For the coherent manipulation of the spins, an electronic pulses system has been developed, based on CPLD (Complex Programmable Logic Device, mod. epm570). This board is controlled by a LabView program that permits to set the length and the delay time between two pulses. The digital signal is converted into an analogue one through a PIC (Peripheral Interface Controller). This pulse is sent to the epm570 and using the RF generator (mod. Tektronix AFG1062), the board is able to produce 3 different types of pulses, as shown in Figure 2.9. The first pulse is the one that excites the sample. The second one going to the switch permits to turn it on/off while the last one is used to triggering the excitation signal. The system is depicted in 2.8.

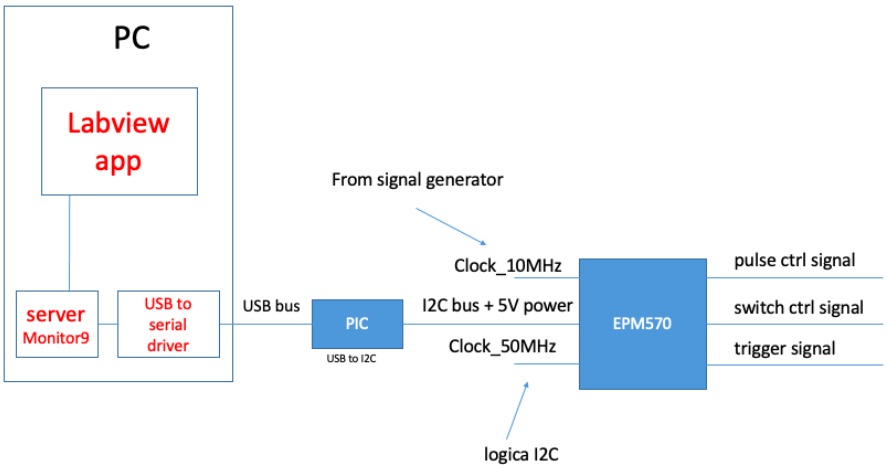

Figure 2.8: Schematic view of the electronic pulses system [made by Franco Gonella].

In Figure 2.9 there is the pulse sequence in time, the opening of the RF input which let the pulse pass and the trigger level of the signal.

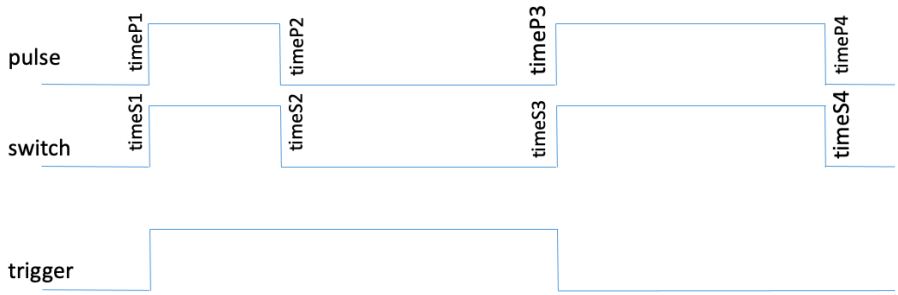

Figure 2.9: Time-signal graphic in the different part of the circuit [made by Franco Gonella].

2.4 Switch

The switch is the device that allows us to use only one RLC circuit to create the magnetic field B_1 and acquire the signal induced by the spins of the sample.
We used a solid-state switch (mod. ZASWA-2-50DRA +), with rise and decay time close to about 20 ns, much shorter than the typical decay times in the experiments carried out in this thesis work. The switch is connected to the EPM570 PCB board and, when the pulses end, it closes the RF gate, making an isolation of 85 dB, as detailed in the data sheet.

Figure 2.10: Switch (mod. ZASWA-2-50DRA +) allows one to use only one wire, to send pulses, and acquired induce voltage. It is possible to see the RF input that represents the connection between the RLC circuit and the gate. The first output is connected to the board for the impulses while the other one is attached to the amplifier and the oscilloscope. The switch is powered by 10 V and the TTL input, also connected to the EPM570, is used to activate the switch.

3 Results

In this section, the previously described pulsed NMR apparatus is used to measure T_2 e T_2^* of a glycerin sample with volume V=(0.8 ± 0.1)cm^3.
As T_1 >> $T2$ in the present sample, we can also assess the inhomogeneity of the magnetic field throughout the sample. We can determine it in two ways:

- by direct calculation, once T_2^* and T_2 have been measured with the FID signal and the pulse echo respectively $\Delta B = \frac{1}{\gamma}\left(\frac{1}{T_2^*} - \frac{1}{T_2}\right)$
- we fit with a Gaussian and Lorentzian the peak in the calculated Fourier Transform of the FID signal. The width of the curve $\Delta\nu$ observed is related to as $\Delta B = \frac{\Delta\nu}{\gamma}$

3.1 Measurement of T_2^*

As described in the previous section, it is possible to obtain a FID signal which in turns gives T_2^* by applying a $\pi/2$ pulse. The correct length of the $\pi/2$ pulse is the one that maximises the FID amplitude. The output of the oscilloscope is presented in Figure 3.1.

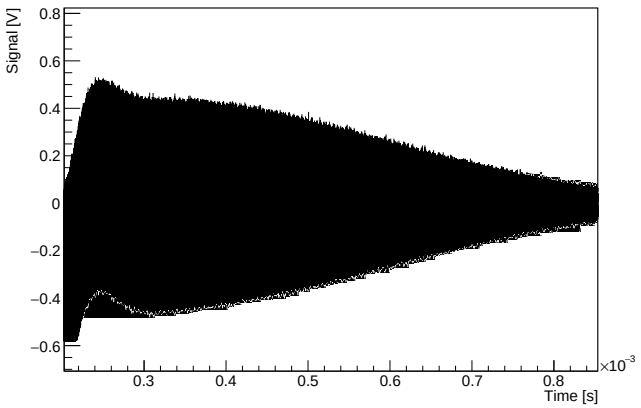

Figure 3.1: Oscilloscope's view of the FID.

Clearly, the observed signal deviates from the expected exponential decay $M_{x,y} = M_{x,y;0}e^{-\frac{t}{T_2^*}}$.
The reason of this difference between theory and experiment can be found in:

- RF signal passes through the closed gate due to insufficient isolation of the switch, which overlaps the FID.
- Impedance matching: as seen before, the system is over-coupled and it causes a sprain of the pulse.

This systematic error is seen in the time domain as a beating signal, as shown in Figure 3.2.

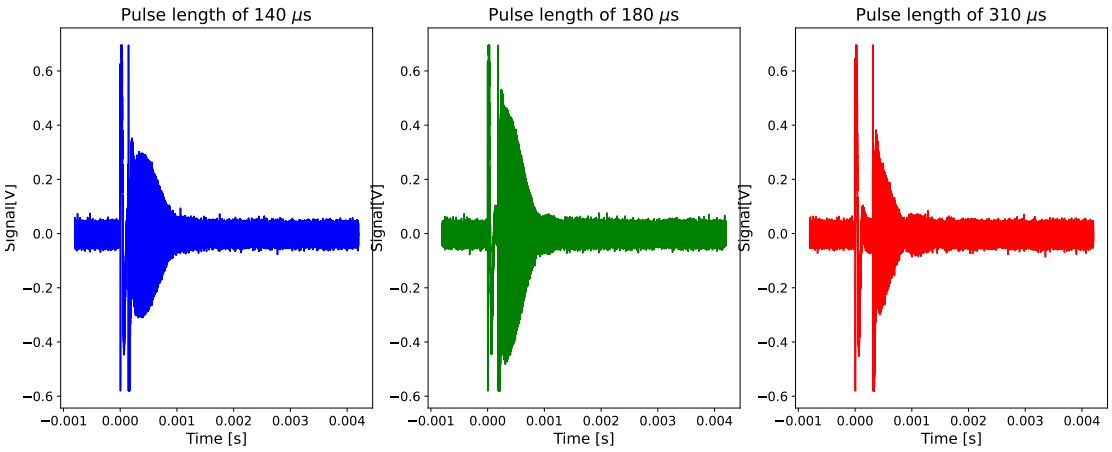

Figure 3.2: View of the systematic error in time domain.

To overcome the beating signal, it is possible to implement the circuit adding another switch synchronized with the other, making a more efficient isolation of the RF gate. In addition, a variable capacitor with a precise setting of its value will be a good choice to overcome the impedance matching.
To determine T_2^*, it is possible to determine the envelope of the signal in a time range between 0.45 ms and 0.6 ms. This procedure is reported in Figure 3.3.

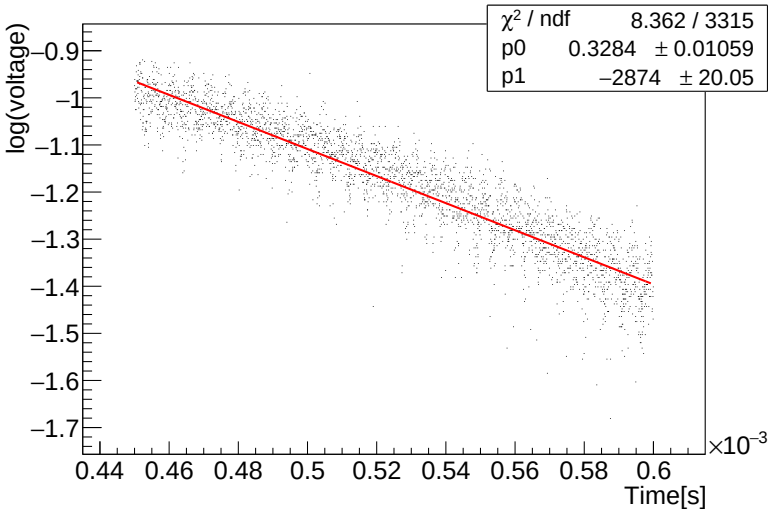

Figure 3.3: Linear fitting on the envelope of FID for the measurement of T_2^*.

The value of T_2^* is $(347 \pm 2)\mu$s.

3.2 Measurement of T_π

To experimentally find T_π, the maximum amplitude of the FID signal should be measured for different durations of the driving pulse. The idea of the works that we want to make is inspired by Figure 3.4 made by Gabrielse and his collaborators [5].

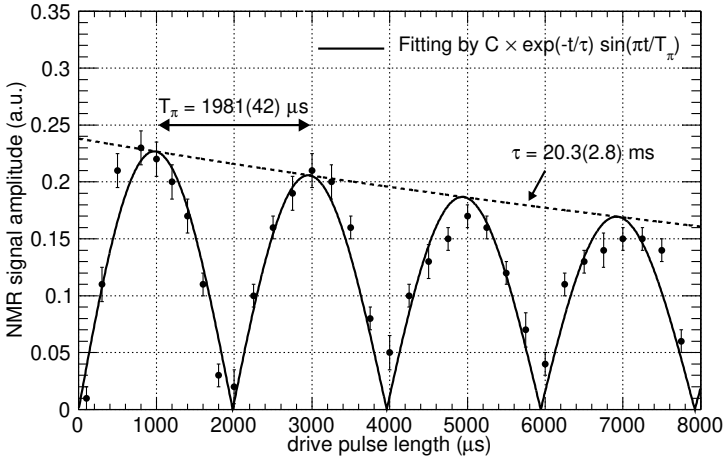

Figure 3.4: Pulse length vs maximum value of FID: a graph for the measurement of the π pulse length presented in [5].

As previously shown, in our case this method would be affected by a large systematic error due to the observed mismatches. The results obtained by plotting the area of the signal vs pulse drive length are shown in Figure 3.5. The signal is fitted by the function:

$$\text{amplitude} = A \cdot \exp^{-\frac{t}{\tau}} \left| \sin\left(\pi \frac{t}{T_\pi}\right) \right| + c$$

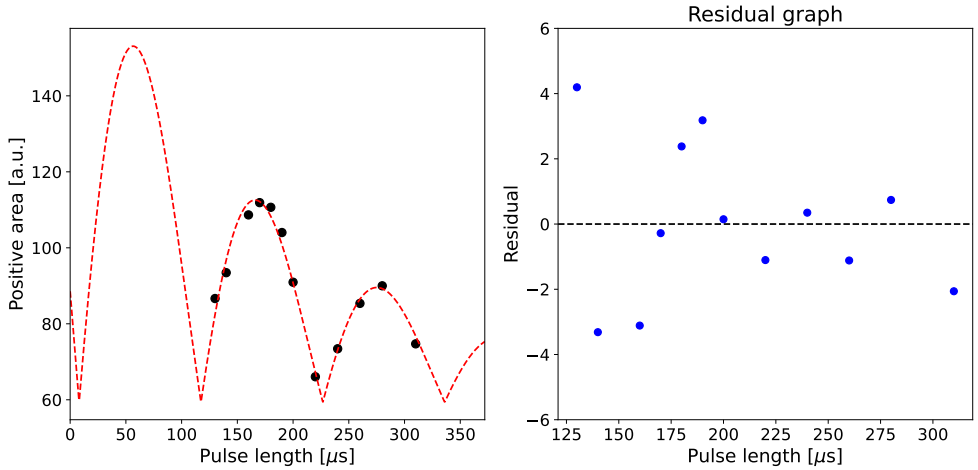

Figure 3.5: Pulse length vs area: a graph for the measurement of the π pulse length. The matching between data and the signal is quite good. The result is $T_\pi = 110\mu$s, completely different to the experimental one.

The π pulse length is about $T_\pi = 110$ μs, completely different from the experimental one which is 360 μs. The calculated value is unrealistic due to systematic error and the small amount of data taken.
In a precedent version of the apparatus, some students have applied the same method using instead the maximum value of the FID, as shown in Figure 3.6.

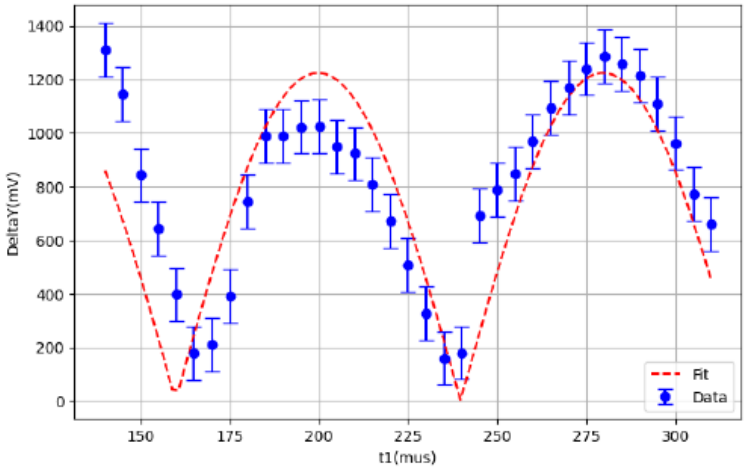

Figure 3.6: Pulse length vs maximum value of the FID: the graph is affected by systematic error because there is an exponential increasing rather than an exponetial decay.

Also in this case the systematic error is present, making the T_π unrealistic. In fact, there is exponential increasing of peaks in the place of an exponential decreasing.

3.3 Measurement of T_2

To determine the value of T_2, it has been used the spin-echo technique already mentioned in section 1.4.4. The magnitude of the signal has been made considering the peak to peak length of the spin echo and the fit is presented in Figure 3.7.

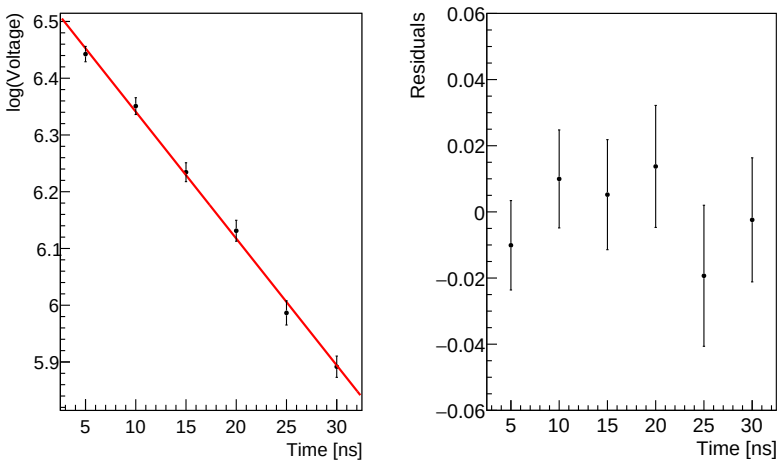

Figure 3.7: Linear $y = p_0 + 2x \cdot p_1$ fitting for the measurement of T_2 which is the inverse of the slope p_1.

The linear fit is appropriated for data, obtaining $T_2 = (89 \pm 3)$ms. From [11], it is possible to determine the concentration of glycerin which is 40 %.

3.4 Measurement of ΔB

Using the first method mentioned before, the field inhomogeneity is:

$$\Delta B_1 = (6.75 \pm 0.04) \cdot 10^{-5}\text{T}$$

In the second option, the FFT of the signal has been made using the library periodogram of *scipy.signal* and the fit's parameters uncertain are given by the program, so they are comprehensive of statistical and computational errors. The fit functions are the Gaussian and Lorentzian respectively:

$$y = A \exp\left(-\frac{(\nu - \nu_0)^2}{2\sigma^2}\right) + c$$

$$y = \frac{A}{(\nu - \nu_0)^2 + \left(\frac{\Delta\nu}{2}\right)^2} + c$$

where c represents an of background's offset. The fits are shown in Figure 3.8 and 3.9 .

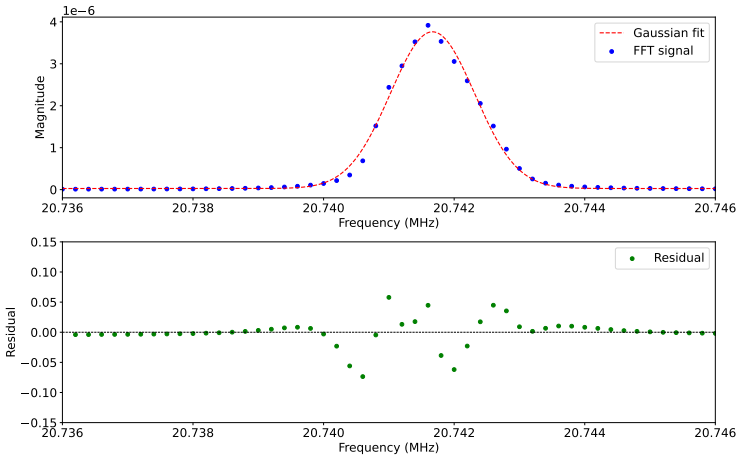

Figure 3.8: Gaussian fit for the ΔB measurement: in the peak, there is a mismatch between Gaussian and data.

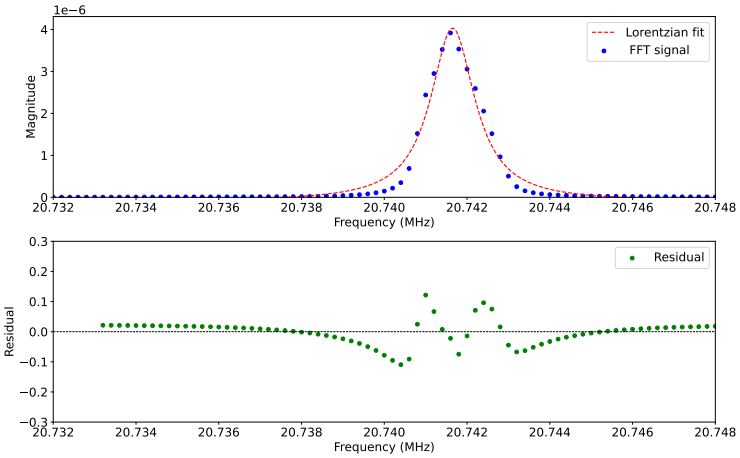

Figure 3.9: Lorentzian fit for the ΔB measurement: in the tail, there is a substantial difference between function and data.

Data are affected to systematic error related to the mismatch, making the fit functions not suitable to them.

Considering the Gaussian fit $\Delta\nu = 2.335 \cdot \sigma$, the field inhomogeneity is $\Delta B_2 = (3.54 \pm 0.05) \cdot 10^{-5}$T while in the Lorentzian one $\Delta B_3 = (3.05 \pm 0.02) \cdot 10^{-5}$T.
The mean value is $\overline{\Delta B} = (3.76 \pm 0.02) \cdot 10^{-5}$T which is compatible to the value declared in the EM data (10^{-5}T with a magnetic field of 0.1 T).

4

Conclusions

The pulsed NMR apparatus that is analysed in this thesis work is located at Laboratori Nazionali di Legnaro (LNL) in Padua and is used for the laboratory of master degree. The NMR sample (diluted glycerin) is located inside the inductance of the RLC circuit, which, in turn, is inside the electromagnet. The other parts of the apparatus are the switch, amplifiers, and pulse generator. This last component is an electronic system that permits to generate two RF pulses setting their length with a delay between them.

The RLC circuit is essential for the apparatus because it allows excitation of the NMR sample and measurement of the induced signal using the same circuit with a solid-state switch. To maximise energy transfer, it is important to characterise the resonant frequency, the bandwidth, and the impedance matching to the line (50 Ω). All of these quantities can be estimated by sending RF pulses through the circuit and analysing the reflected signal using a directional coupler. When the reflected signal is minimised and the RF exponential decay is rapid, the resonant frequency and impedance matching are achieved. In this thesis, this procedure has been used with and without the NMR sample. It is obtained, with the sample inside the wire, a overlapped system with resonant frequency of 20.740 MHz and a quality factor of 31 ± 1.

In the pulsed NMR is necessary to set the Larmor frequency the same of the resonant one using a static B-field produced by the electromagnet of $B = \nu_0/\tilde{\gamma} = 0.487\text{T}$ where $\tilde{\gamma} \approx 42.576\text{MHz/T}$, which requires a current of 7.832 A. To test the operation's correctness of the apparatus, the T_2^*,T_2 and ΔB of the electromagnet are measured. All of this result are subjected to a considerable systematic error related to the mismatching impedance and imperfect isolation of the switch. Performing the exponential fit $M_{x,y} = M_{x,y;0}e^{-\frac{t}{T_2^*}}$ in the envelope of the FID in a certain time range, the result is $T_2^* = (347 \pm 2)\mu\text{s}$. For the estimation of T_2, it is necessary to use the spin echo sequence consisting of a pulse $\pi/2$ and a pulse π with a delay between them; only in this way is possible to remove the effects of field inhomogeneity. The result of the spin echo exponential fit $M_{x,y} = M_{x,y;0}e^{-\frac{t}{T_2}}$ is T_2=(89 ± 3)ms.

For the field inhomogeneity, there are two possible ways of calculating: the first is to apply $\Delta B = \frac{1}{\gamma}\left(\frac{1}{T_2^*} - \frac{1}{T_2}\right)$ using the precedent result of T_2 and T_2^*. The result is $\Delta B_1 = (6.75 \pm 0.04) \cdot 10^{-5}\text{T}$. Secondly, there is the possibility of fitting the Fourier transformation of the FID with a Gaussian or Lorentzian function, obtaining, respectively, $\Delta B_2 = (3.54 \pm 0.05) \cdot 10^{-5}\text{T}$ and $\Delta B_3 = (3.05 \pm 0.02) \cdot 10^{-5}\text{T}$. The mean value is $\overline{\Delta B} = (3.76 \pm 0.02) \cdot 10^{-5}\text{T}$, compatible with the one declared by the electromagnet constructor.

References

[1] Jim Napolitano Adrian C. Melissinos. *Experiments in Modern Physics*. Academic Press, 2003.

[2] F. Bloch. "Nuclear Induction". In: *Phys. Rev.* 70 (7-8 Oct. 1946), pp. 460–474. DOI: 10.1103/PhysRev.70.460. URL: https://link.aps.org/doi/10.1103/PhysRev.70.460.

[3] Franck Laloe Claude Cohen-Tannoudji Bernard Diu. *Quantum Mechanics, Volume 1: Basic Concepts, Tools, and Applications*. Wiley-VCH, 2019.

[4] Eric R.Dietz Darly W.Preston. *The art of experimental physics*. John Wiley sons, 1991.

[5] X. Fan, S. E. Fayer, and G. Gabrielse. "Gaseous 3He nuclear magnetic resonance probe for cryogenic environments". In: *Review of Scientific Instruments* 90.8 (Aug. 2019). ISSN: 1089-7623. DOI: 10.1063/1.5099379. URL: http://dx.doi.org/10.1063/1.5099379.

[6] University of Florida-Department of Physics. *Pulsed Nuclear Magnetic Resonace*. URL: https://www.phys.ufl.edu/courses/phy4803L/group_II/nmr/nmr.pdf. (accessed: 24.07.2024).

[7] E. L. Hahn. "Free nuclear induction". In: *Physics Today* 6.11 (Nov. 1953), pp. 4–9. ISSN: 0031-9228. DOI: 10.1063/1.3061075. eprint: https://pubs.aip.org/physicstoday/article-pdf/6/11/4/8317838/4_1_online.pdf. URL: https://doi.org/10.1063/1.3061075.

[8] Jeremiah Holzbauer. *RF Theory and Design-Notes*. URL: https://uspas.fnal.gov/materials/12MSU/RF_Design_Lecture_Notes.pdf. (accessed: 24.07.2024).

[9] Piter Kok. *Advanced Quantum Mechanis*. URL: https://phys.libretexts.org/@go/page/56547.

[10] Mit Department of Physics. *Pulsed Nuclear Magnetic Resonace:Spin Echos*. URL: https://web.mit.edu/8.13/www/JLExperiments/JLExp12.pdf. (accessed: 24.07.2024).

[11] Muye "Willers" Yang. *Measuring T2 of diluted Glycerin as a Function of Concentration*.